Article

Conjugated Polymer Nanoparticles Based on Anthracene and Tetraphenylethene for Nitroaromatics Detection in Aqueous Phase

Tianwen Ouyang [1], Xue Guo [1], Qihao Cui [1], Wei Zhang [1], Wenyue Dong [1],* and Teng Fei [2],*

[1] School of Materials Science and Engineering, Changchun University of Science and Technology, Changchun 130022, China
[2] State Key Laboratory of Integrated Optoelectronics, College of Electronic Science and Engineering, Jilin University, Changchun 130012, China
* Correspondence: dongwenyue@cust.edu.cn (W.D.); feiteng@jlu.edu.cn (T.F.)

Abstract: The sensitive and selective detection of nitroaromatic explosives is of great significance to national security and human health. Herein, the novel linear polymer *l*-PAnTPE and cross-linked polymer PAnTPE nanoparticles based on anthracene and tetraphenylethene groups were designed and successfully synthesized via Suzuki-miniemulsion polymerization. The particle sizes of the polymers are around 73 nm, making them well dispersible in water. The cross-linked polymer PAnTPE exhibits porous structure, which is beneficial for the diffusion/adsorption of analytes. The fluorescence sensing towards nitroaromatics was performed in the aqueous phase, and *l*-PAnTPE and PAnTPE nanoparticles showed different quenching degree towards different nitroaromatics. Among them, the quenching constant K_{SV} values of *l*-PAnTPE and PAnTPE towards 2,4,6-trinitrophenol (TNP) reach 1.8×10^4 M^{-1} and 4.0×10^4 M^{-1}, respectively, which are 1–2 orders of magnitude higher than other nitroaromatic explosives, thus demonstrating the high sensitivity and selectivity of TNP detection in the aqueous phase. The sensing mechanism was further discussed to clarify this phenomenon by analyzing UV–Vis absorption, excitation, fluorescence spectra, cyclic voltammograms and fluorescence decay measurements. In addition, the paper strips tests exhibit that *l*-PAnTPE and PAnTPE have great potential in the application of fast, low-cost and on-site nitroaromatics detection.

Keywords: explosive detection; fluorescence sensing; polymer nanoparticles; TNP detection

1. Introduction

Nitroaromatic explosives, such as 2,4,6-trinitrophenol (TNP, also called picric acid), 1,3,5-trinitrobenzene (TNB) and 2,4-dinitrotoluene (DNT), etc., have been used to prepare rocket fuels, leather and pharmaceutical intermediates, especially bombs. Due to their explosive capacity and high toxicity, the widespread use of nitroaromatics threatens global security, causes serious environmental pollution and is harmful to human health, causing skin, eye irritation and chronic diseases [1–3]. The nature of nitroaromatics highlights the demand for sensitive and selective detection technology [4,5]. So far, there are many methods developed for nitroaromatics detection, including liquid chromatography–mass spectroscopy (LC–MS) [6], ion mobility spectroscopy [7], gas chromatography–mass spectroscopy (GC–MS) [8], high performance liquid chromatography (HPLC) [9], proton transfer reaction mass spectroscopy (PTR–MS) [10], surface plasmon resonance (SPR) [11], electrochemical analysis [12], surface enhanced Raman scattering (SERS) [13] and so on. However, these technologies have some limitations, such as complicated sample pretreatment, expensive instruments, strict operation and inadequate portability. Photoluminescence (PL) sensing owns the advantages of low cost, high sensitivity, fast response and on-site detection, becoming a popular method for nitroaromatics detection [14–17]. To date, the main materials used for PL sensing include small molecules based fluorophores [18,19],

quantum dots (QDs) [16,20], metal-organic frameworks (MOFs) [21–23], conjugated polymers (CPs) [24–27] and so on [28–30].

Conjugated polymers can amplify fluorescent signals due to the 'molecular wire' effect, which could improve the sensitivity of PL detection [31]. There are many kinds of conjugated polymers developed for PL sensing, including hydrophobic conjugated polymers, hydrophilic conjugated polymers, conjugated porous polymers, etc. For example, Hua et al. prepared a diketopyrrolopyrrole-based conjugated polymer, which shows good sensitivity and low cytotoxicity for the detection of fluoride ion and cell bioimaging [32]. Ramanavicius et al. combined the conducting polymer polypyrrole (Ppy) with bovine leukemia virus protein *gp51* to detect specific antibodies (anti-*gp*51-Ab), with an increase in the selectivity of the immunosensor by application of Ppy. [33]. Cui et al. synthesized a novel conjugated polymer with hydroxyl groups, which was used to detect DNT and TNT in aqueous phase with the limits of detection of 7.4×10^{-7} mol/L and 1.1×10^{-6} mol/L, respectively [34]. Qin and Liang et al. reported a fluorescence probe TPE-SFX based on tetraphenylethene (TPE) modified spiro(fluorene-9,9′-xanthene) (SFX), and the prepared TPE-SFX paper strips showed good performance, with the detection limit of 0.12 nmol/cm^2 for TNP [35]. He et al. reported a conjugated porous polymer, based on triphenylamine (TPA) and 2,2′-bipyridine, which realized a high sensitivity for the detection of Fe^{3+} and Fe^{2+} ions [36]. Dong et al. synthesized a conjugated polyfluorene derivative (PCFSe) with benzo[c][1,2,5]selenadiazole in polyfluorene backbone and N-alkylcarbazole in the side chain, and PCFSe, as a fluorescent sensor, exhibited varying degrees of fluorescence quenching towards different nitroaromatics, in which picric acid (PA) detection has the highest sensitive response with a K_{SV} value of 1.2×10^4 M^{-1} and the calculated detection limit of 0.27 ppm in THF [37]. However, most conjugated polymers, except for hydrophilic conjugated polymers, are hardly soluble or well-dispersible in pure water, which may limit their application in aqueous media.

To solve this problem, the emergence of water-dispersible polymer nanoparticles opens up the possibility for nitroaromatics detection in the aqueous phase. For example, Tang et al. synthesized aggregation-induced emission (AIE)-active hyperbranched poly(2,5-silole)s for the first time in high yields (up to 98%) and the nano-aggregates (in a THF/H_2O mixture) displayed a fluorescence response to TNP, giving a detection limit of 1 ppm of TNP in the THF/H_2O [38]. Sengottuvelu and Laskar et al. synthesized aggregation-induced enhanced emission (AIEE)-active conjugated mesoporous oligomers containing TPA and TPE and their nanoaggregates were prepared and used for nitroaromatics detection in quasi-aqueous solution at f_w = 90% (in water/THF) [39]. Kim et al. synthesized a hyperbranched conjugated polymer by polycondensation of TPE and hyperbranched polyglycidol (HPG) with an average diameter of 100 nm for the detection of nitroaromatics in the aqueous phase, and the detection limit of TNP was 40 ppb [25]. Tong and Wang et al. prepared water-dispersible hyperbranched conjugated polymer nanoparticles (HCPN-S) for the highly sensitive detection of TNT in pure water [40]. Patra et al. fabricated conjugated porous organic polymer nanoparticles based on a novel core of tetraphenyl-5,5-dioctylcyclopentadiene (TPDC) and applied them for the sensing of nitroaromatics in water with K_{SV} of 7.6×10^4 M^{-1} towards TNP [41]. Duan and Fei et al. synthesized a cross-linked poly(triphenylamine-co-benzothiadiazole)s (PTPABT) with a particle size of 40–70 nm, which possessed good dispersion in aqueous phase and showed high sensitivity for TNB detection in pure aqueous phase with a detection limit of 1.9×10^{-5} M [42]. Cao and Zhao et al. prepared an AIE cross-linked poly(DVB-co-TPE-PBE) nanoparticles by copolymerization in a water-borne miniemulsion system, and the sensitive detection of nitroaromatics in the aqueous phase was realized, especially for highly sensitive and selective detection towards TNP with a K_{SV} value of 2.65×10^4 M^{-1} [43]. Zhou and Zhao et al. reported a series of neutral conjugated polymers (NCPs) containing TPE, which could function as fluorescent probes to detect TNP in aqueous media with extremely high sensitivity, low detection limit and good anti-photobleaching properties [44].

In this work, linear polymer (*l*-PAnTPE) nanoparticles and cross-linked polymer (PAnTPE) nanoparticles based on typical AIE-active TPE groups and electron-rich anthracene (An) moieties were designed and successfully synthesized by Suzuki-miniemulsion polymerization. The polymers show spherical particle morphologies with particle size of ca. 73 nm, and cross-linked PAnTPE exhibits porous characteristics with pore size centered at ca. 3.5 nm, which is beneficial to construct the channels for analyst adsorption and diffusion. The PL detection of nitroaromatics was performed by PL titration experiments in water, and the detection of TNP with high sensitivity and selectivity was realized. Furthermore, the paper strips based on our polymers were fabricated, and the practical application of rapid, low cost and on-site detection of TNP was achieved. Our research data demonstrate that an efficient PL sensing performance towards TNP in aqueous phase could be obtained through the structural design and preparation of conjugated polymer nanoparticles.

2. Experimental

2.1. Reagents and Measurements

The details of reagents and measurements are given in Supplementary Information (SI).

2.2. Synthesis

2.2.1. 9,10-Bis(4,4,5,5-tetramethyl-1,3,2-dioxaborolan-2-yl)anthracene (An-2B)

A mixture of 9,10-dibromoanthracene (2.02 g, 6.00 mmol), bis(pinacol)diboron (3.66 g, 14.40 mmol), potassium acetate (3.53 g, 36.00 mmol) and Pd(dppf)Cl$_2$ (0.12 g, 0.15 mmol) were carefully degassed and then dissolved in DMF (20 mL). The mixture was stirred at 90 °C for 24 h under nitrogen atmosphere. After cooling to room temperature, the mixture was treated with water and extracted with chloroform. The organic phase was collected and dried over anhydrous MgSO$_4$. The crude product was purified by column chromatography to give the polymer as a white solid in 46% yield (1.18 g). ^{1}H NMR (400 MHz, C$_2$D$_2$Cl$_4$): δ = 8.31 (dd, J = 3.3, 6.7 Hz, 4H), 7.49 (dd, J = 3.3, 6.8 Hz, 4H), 1.58 (s, 24H). ^{13}C NMR (100 MHz, C$_2$D$_2$Cl$_4$) δ 135.04, 129.18, 125.55, 84.90, 25.49. MS m/z: calcd., 430.16; found 430.72.

2.2.2. *l*-PAnTPE Nanoparticles

Sodium dodecyl sulfate (SDS) (0.20 g, 0.69 mmol) and K$_2$CO$_3$ (0.25 g, 1.80 mmol) were dissolved in deionized water (20 mL), then ultrasonically treated for 15 min. An-2B (0.13 g, 0.30 mmol), TPE-2Br (0.15 g, 0.30 mmol) and tetrakis(triphenylphosphine)palladium (Pd(PPh$_3$)$_4$, 0.01 g, 0.01 mmol) were dissolved in toluene (2 mL). The water phase was added to the organic phase and treated ultrasonically for 10 min to form a stable miniemulsion. The obtained miniemulsion was degassed three times and heated at 85 °C for 24 h. Finally, the solution was packed in dialysis bag (Mn 3500 g/mol) for dialysis to remove the surfactants and unreacted monomers. The linear polymer *l*-PAnTPE nanoparticles were obtained in 32% yield.
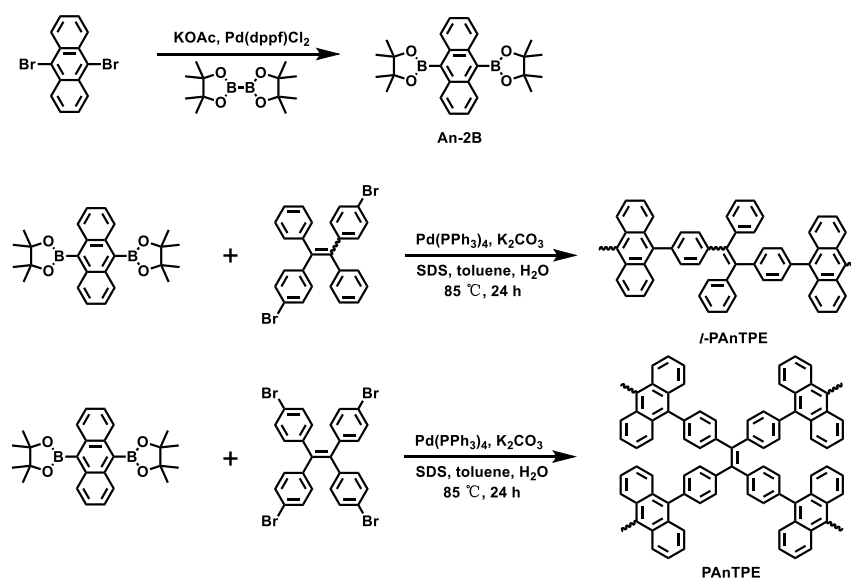
2.2.3. PAnTPE Nanoparticles

SDS (0.20 g, 0.69 mmol) and K$_2$CO$_3$ (0.25 g, 1.80 mmol) were dissolved in deionized water (20 mL), then ultrasonically treated for 15 min. An-2B (0.13 g, 0.30 mmol), TPE-4Br (0.10 g, 0.15 mmol) and Pd(PPh$_3$)$_4$ (0.01 g, 0.01 mmol) were dissolved in toluene (2 mL). The water phase was added to the organic phase and treated ultrasonically for 10 min. The obtained miniemulsion was degassed three times and heated at 85 °C for 24 h. Finally, the solution was packed in dialysis bag (Mn 3500 g/mol) for dialysis to remove the surfactants and unreacted monomers. The cross-linked polymer PAnTPE nanoparticles were obtained in 35% yield.

3. Results and Discussion

3.1. Synthesis and Characterization

Scheme 1 illustrates the synthesis routes to *l*-PAnTPE and PAnTPE nanoparticles. The monomers of dibromo-substituted TPE (TPE-2Br) and tetrabromo-substituted TPE (TPE-4Br) were synthesized by McMurry coupling reaction according to the literature [39]. An-2B was synthesized by Suzuki-Miyaura reaction. *l*-PAnTPE and PAnTPE nanoparticles were prepared by Suzuki coupling in toluene/water miniemulsion. The chemical structures of the obtained polymers were successfully confirmed by FT–IR spectra. In Figure 1a, for *l*-PAnTPE, the peak at 2928 cm^{-1} is attributed to the C–H stretching of the phenyl rings. The peaks at 1650 and 1543 cm^{-1} are attributed to the C=C stretching of the phenyl rings. The peak at 700 cm^{-1} comes from the C–H bending of the phenyl rings. In Figure 1b, for PAnTPE, the peaks at 2979 and 2929 cm^{-1} are attributed to be the C–H stretching of the phenyl rings. The C=C stretching of the phenyl rings occur at 1486 and 1415 cm^{-1}. The peaks at 1314–758 cm^{-1} come from the C–H bending of the phenyl rings. It is worthwhile noting that the C–Br vibration peaks at 591 cm^{-1} and 503 cm^{-1} from the monomers TPE-2Br and TPE-4Br almost completely disappear, indicating that the Suzuki coupling reactions were completed [45,46].

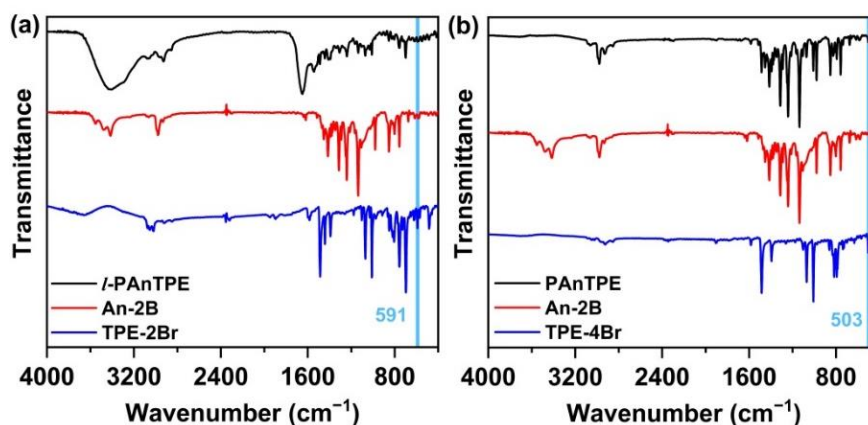**Scheme 1.** Synthesis routes to *l*-PAnTPE and PAnTPE nanoparticles.

Figure 1. FT–IR spectra of *l*-PAnTPE (**a**), PAnTPE (**b**) and the corresponding monomers.

Scanning electron microscope (SEM) images, transmission electron microscope (TEM), dynamic light scattering (DLS) and nitrogen sorption isotherms were obtained for the

characterization of the morphologies and porosities of the polymers. As shown in Figure 2, the uniform particles of *l*-PAnTPE and PAnTPE can be observed from the SEM images, and the average particle sizes are ca. 73 nm for both polymers. TEM images of *l*-PAnTPE and PAnTPE are shown in Figure S1; compared with SEM, spherical particles are also obtained with similar particle sizes. Figure S2 shows the DLS analysis of the nanoparticles, and the average hydrodynamic diameters of *l*-PAnTPE and PAnTPE were measured as ca. 60 nm and 84 nm, respectively. The nanoparticle morphologies of *l*-PAnTPE and PAnTPE guarantee their good dispersity in water. The specific surface area and pore size were obtained by nitrogen sorption isotherms. As shown in Figure 3, the cross-linked polymer PAnTPE shows a hysteresis loop in the range of $P/P_0 = 0.03$–1, and the curve indicates the characteristics of the IV type isotherm curve. The Brunauer-Emmett-Teller (BET) surface area of PAnTPE was determined to be 49.3 m^2/g, and the pore size distribution is centered at ca. 3.5 nm. In contrast, the BET surface area of *l*-PAnTPE is zero due to its linear structure. The porous nature of the cross-linked polymer PAnTPE can provide a channel for the adsorption/diffusion of explosive molecules in the polymer, which is beneficial for the PL sensing towards nitroaromatics.
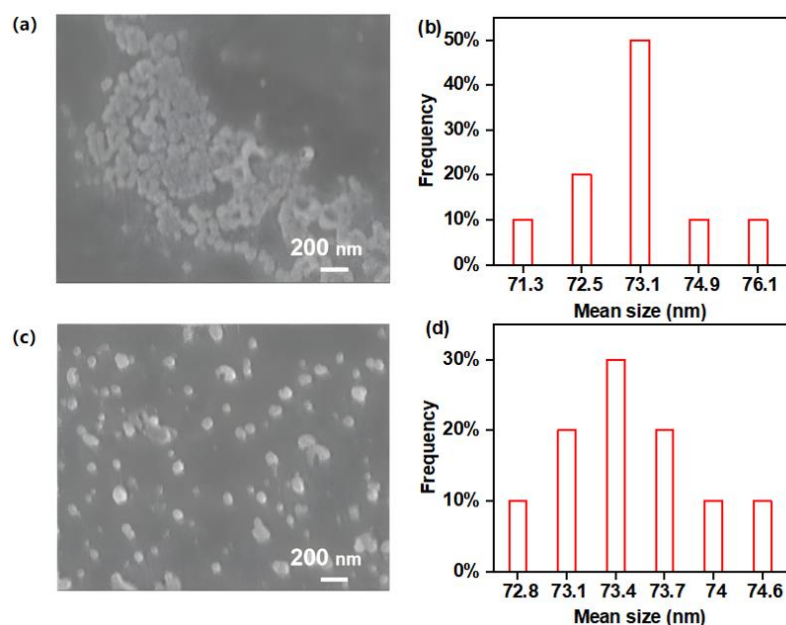

Figure 2. SEM images of *l*-PAnTPE (**a**) and PAnTPE (**c**), and particle size distributions of *l*-PAnTPE (**b**) and PAnTPE (**d**).
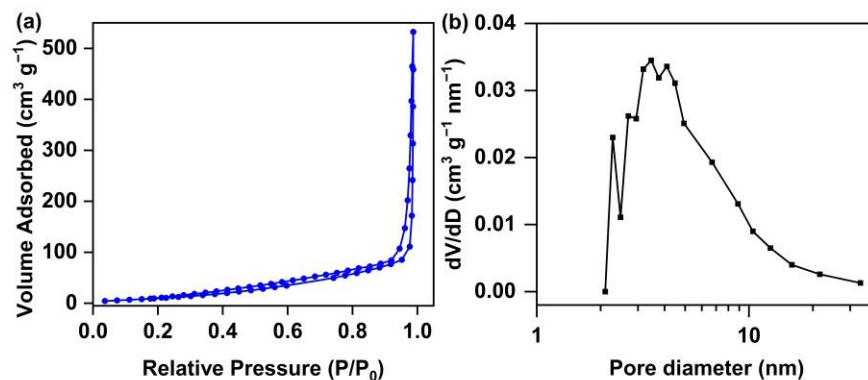

Figure 3. The nitrogen isothermal adsorption desorption curves (**a**) and pore size distribution (**b**) of PAnTPE.

3.2. Photophysical Properties

The photophysical properties of the *l*-PAnTPE and PAnTPE were characterized by UV–Vis and emission spectra in aqueous media. As shown in Figure 4a,b, the UV–Vis spectrum of *l*-PAnTPE exhibits an absorption peak at 257 nm and a shoulder peak near 373 nm, while PAnTPE exhibits a strong absorption peak at 257 nm and a shoulder peak at 333 nm, which are corresponding to the π–π* transition of An and TPE groups. The emission spectra show a maximum excitation wavelength and a maximum emission wavelength at 393 nm and 455 nm for *l*-PAnTPE, 336 nm and 448 nm for PAnTPE, respectively. From the CIE, *l*-PAnTPE and PAnTPE in water both exhibit blue emission (Figure 4c,d). Compared with the linear polymer *l*-PAnTPE, the emission peak of the cross-linked polymer PAnTPE has a ca. 7 nm blue shift, which is possibly due to the stronger rigidity and conjugation from the cross-linked structure.
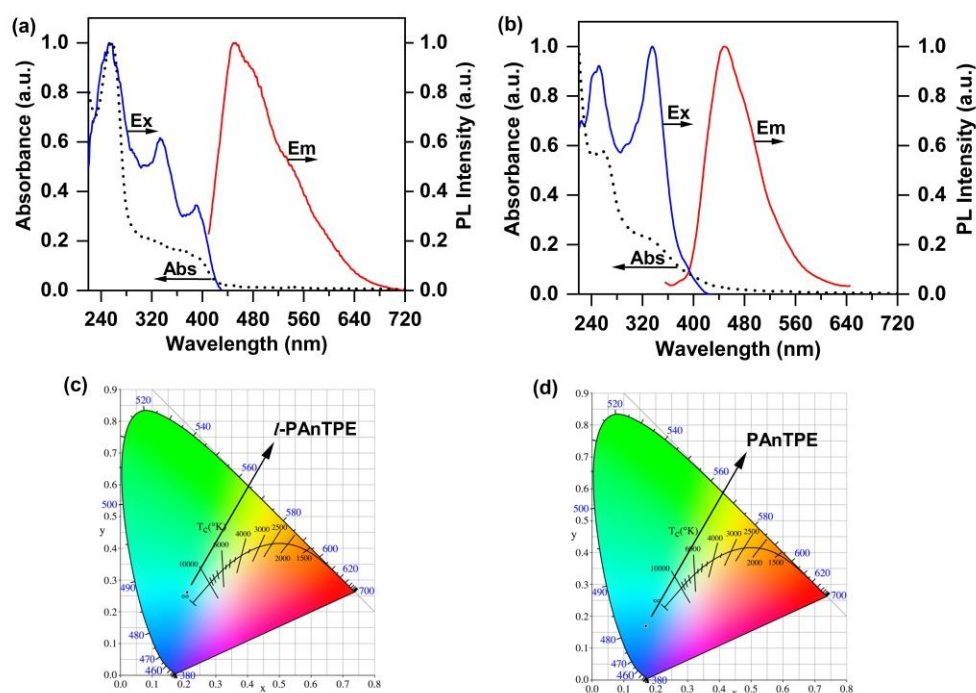

Figure 4. The excitation spectra, UV–Vis absorption spectra and emission spectra of *l*-PAnTPE (**a**) and PAnTPE (**b**) in water. CIE of *l*-PAnTPE (**c**) and PAnTPE (**d**) in water.

3.3. Nitroaromatics Detection

Because of good dispersion of the obtained polymers in water, *l*-PAnTPE and PAnTPE could be used to detect nitroaromatics in aqueous phase. The PL spectra with different amounts of TNP and the Stern–Volmer (S–V) plots of *l*-PAnTPE and PAnTPE measured in water were recorded in Figure 5. As shown in Figure 5a,c, the polymers *l*-PAnTPE and PAnTPE exhibit apparent PL quenching with increasing TNP concentration, and the PL intensities are quenched almost completely when TNP concentrations reach 183 μM and 142 μM, respectively. Using quinine sulfate as reference, the PL quantum yields of *l*-PAnTPE and PAnTPE aqueous dispersion were calculated to be ca. 1.8% and 2.0% in the absence of TNP and decreased to ca. 0.040% and 0.060% after the addition of 183 μM and 142 μM of TNP, respectively. It is noteworthy that the PL spectra show no obvious change after adding TNP, which means that no other emissive species were formed during the quenching process. To calculate the quenching efficiency of *l*-PAnTPE and PAnTPE in response to TNP concentration in water, S–V plots were obtained using the equation ($I_0/I = 1 + K_{SV}$ [Q]); here, I_0 denotes emission intensity of polymers without any quencher, I denotes the emission intensity of polymer with quencher with concentration [Q], and K_{SV} represents the S–V quenching constant (M^{-1}). In Figure 5b,d, the K_{SV} values of *l*-PAnTPE and PAnTPE

were determined to be 1.8×10^4 M^{-1} and 4.0×10^4 M^{-1}, respectively, demonstrating a sensitive PL sensing towards TNP. In addition, the other two important parameters, the limit of detection (LOD) and limit of quantification (LOQ) values, were calculated as 663 nM and 2.20 μM for *l*-PAnTPE, 439 nM and 1.50 μM for PAnTPE, respectively, via the equation LOD = 3 σ/m and LOQ = 10 σ/m, where σ is the standard deviation of the PL intensities of the blank solution, and m represents the slope of the linear fitting curve (Figure S3, Tables S1 and S2) [37]. From the K$_{SV}$s, LODs and LOQs, the cross-linked polymer PAnTPE shows higher sensitivity than the linear polymer *l*-PAnTPE, which could be attributed to the porous structure of cross-linked PAnTPE, thus facilitating the contact and the adsorption/diffusion of the analyte in the polymer. For comparison, some literature data of polymer-based PL sensing materials for TNP detection are summarized in Table 1, indicating that *l*-PAnTPE and PAnTPE nanoparticles are very promising for the PL sensing towards TNP detection.
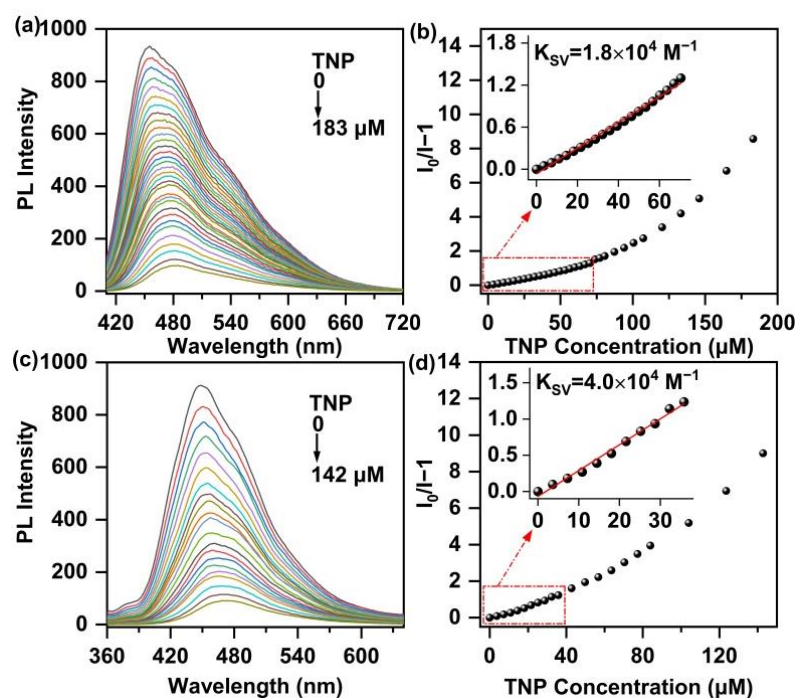

Figure 5. Emission spectra of *l*-PAnTPE (**a**) and PAnTPE (**c**) aqueous dispersion with increasing amounts of TNP. S–V plots of PL intensity (I$_0$/I−1) of *l*-PAnTPE (**b**) and PAnTPE (**d**) vs. TNP concentration.

Table 1. Literature data of polymer materials for TNP detection.

Polymeric Material	Ksv/M^{-1}	LOD	References	Test Environment
l-PAnTPE	1.8×10^4	663 nM	This work	Water
PAnTPE	4.0×10^4	439 nM	This work	Water
P2	2.03×10^4	-	[47]	THF-water
oTPETP	1.64×10^2	0.053 mM (12 ppm)	[48]	THF-water
P1e2c	1.72×10^4	510 nM	[49]	Water
FPP-3	1.64×10^4	59 ppb	[50]	Methanol
DCP	1.6×10^4	3.7 μM	[51]	THF
DVB-co-TPE-PBE	2.65×10^4	5.43 μM (1.24 ppm)	[43]	THF-water
PTPE	1.72×10^7	5 nM	[44]	THF-water
HPG-TPE	2.27×10^4	40 ppb	[25]	THF-water
PFBT	2.18×10^5	0.19 nM	[52]	DMSO
P2	6.40×10^4	525 nM (120 ppb)	[53]	CHCl$_3$
PBEMA	2.45×10^5	0.114 μM	[54]	Water
TTRZ	1.15×10^5	27 ppb	[55]	Methanol

Selectivity is important for the explosives detection, thus the PL quenching experiments of *l*-PAnTPE and PAnTPE towards TNB and DNT were tested as well. From the S–V plots, the K_{SV} values of *l*-PAnTPE toward TNB and DNT were calculated to be 8.8×10^2 M^{-1} and 2.6×10^3 M^{-1}, the LODs were calculated to be 16.6 μM and 6.60 μM, the LOQs were calculated to be 55.2 μM and 22.1 μM, respectively (Figures S4 and S5, Table S1). As for PAnTPE, the K_{SV} values towards TNB and DNT were found to be 3.9×10^3 M^{-1} and 2.2×10^3 M^{-1}, the LODs were calculated to be 3.60 μM and 5.70 μM and the LOQs were calculated to be 11.8 μM and 19.1 μM, respectively (Figures S6 and S7, Table S2). These much lower K_{SV}, LOD and LOQ values indicate high selectivity for TNP detection based on *l*-PAnTPE and PAnTPE. Selectivity of *l*-PAnTPE and PAnTPE towards TNP was also tested in a competitive environment with other nitroaromatic compounds (phenol as comparison) in water. As shown in Figure 6, after adding 35 μM TNP into PAnTPE aqueous dispersion, the PL intensity sharply decreases to 46%. The addition of the same concentration of other explosives causes little effect in the PL intensity of PAnTPE, then the PL intensity decreases significantly upon adding 35 μM of TNP to the similar quenching degree of adding TNP alone. Similar experimental phenomenon could be obtained from *l*-PAnTPE (Figure 6a), and the results indicate a good recognition of TNP based on *l*-PAnTPE and PAnTPE nanoparticles in the presence of other interfering nitroaromatic compounds. In addition, the PL quenching effect was recorded by adding potential interfering ions (Na^+, K^+, Ba^{2+}, Ca^{2+}, Mg^{2+}, Fe^{2+}, Mn^{2+}, Zn^{2+}, OH^-, Fe^{3+}, Cu^{2+}, NO_2^- and Br^-) into *l*-PAnTPE and PAnTPE aqueous dispersions, as shown in Figure S8. It is worth nothing that the interfering ions caused very little effect on the PL of *l*-PAnTPE and PAnTPE dispersion, indicating the high selectivity of TNP detection and anti-interference to the common ions in actual water samples based on the polymer nanoparticles.
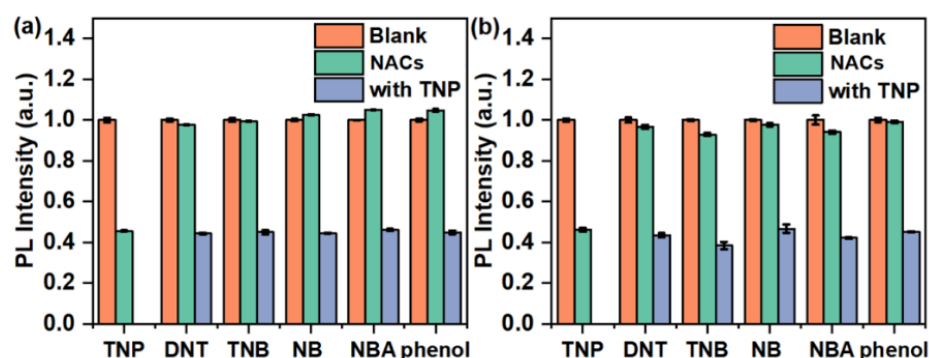

Figure 6. The quenching degree of *l*-PAnTPE (**a**) and PAnTPE (**b**) aqueous dispersion towards different nitroaromatics (NACs) and phenol of 70 μM and 35 μM, respectively, followed by adding the same amount of TNP.

3.4. Quenching Mechanism

The electron-rich structures of the conjugated polymers *l*-PAnTPE and PAnTPE are conductive to their interaction with electron-deficient nitroaromatic explosives, while the porous spherical structure of the cross-linked polymer PAnTPE nanoparticles is more conducive to the adsorption and diffusion of the sensing analytes. Therefore, the PL sensing performance of the cross-linked PAnTPE nanoparticles is better than that of the linear *l*-PAnTPE. In addition, a highly sensitive and selective detection of TNP in pure water was achieved based on *l*-PAnTPE and PAnTPE nanoparticles. To further understand this phenomenon, the PL sensing mechanism between the polymers and nitroaromatics was investigated.

The electrochemical properties of *l*-PAnTPE and PAnTPE were examined by the cyclic voltammogram (CV) curves, as shown in Figure S9. The onset potentials of *l*-PAnTPE and PAnTPE are 1.22 V and 1.15 V, respectively. According to the equation HOMO (highest-occupied molecular orbitals) = $-(E_{Ox}^{onset} + 4.36)$ eV, the HOMO energy levels of *l*-PAnTPE and PAnTPE were calculated to be -5.58 eV and -5.51 eV, respectively. Moreover, from

the UV–Vis absorption spectra of the polymers, the optical band gap E_g was determined to be 2.90 and 2.98 eV for *l*-PAnTPE and PAnTPE, respectively. According to the equation LUMO (lowest-unoccupied molecular orbitals) = HOMO + E_g, the LUMO energy levels of *l*-PAnTPE and PAnTPE were calculated to be −2.68 eV and −2.53 eV, respectively. The LUMO energy levels of *l*-PAnTPE and PAnTPE were higher than that of TNP, TNB and DNT [56,57] (Figure 7), therefore, photoinduced electron transfer process may exist during the PL quenching. In addition, the LUMO energy level of TNP is lower than that of TNB and DNT, which might be one reason for the high sensitivity to TNP detection.
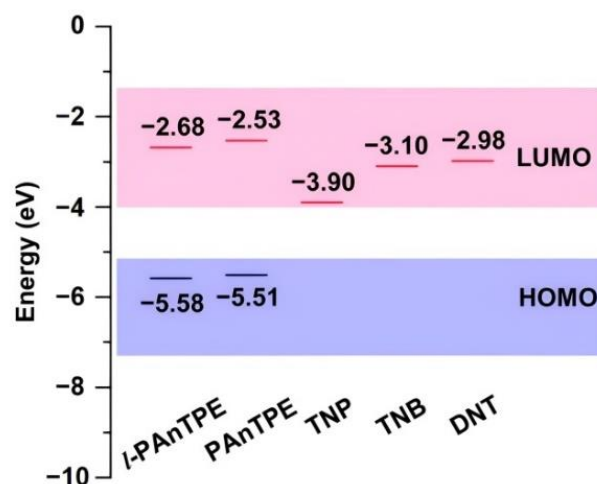

Figure 7. HOMO and LUMO energy levels of *l*-PAnTPE, PAnTPE and nitroaromatic explosives.

Figure 8 shows the excitation and PL spectra of *l*-PAnTPE and PAnTPE nanoparticles and the UV–Vis absorption spectra of nitroaromatics in water. As shown in Figure 8, the UV–Vis absorption spectrum of TNP overlaps with the PL spectra of *l*-PAnTPE and PAnTPE, indicating the possibility of Föster resonance energy transfer mechanism [58]. In addition, the excitation spectra of *l*-PAnTPE and PAnTPE also overlap with the UV–Vis absorption spectrum of TNP to a large extent, so an inner filter effect (IFT) may exist during the PL quenching process with TNP [52].
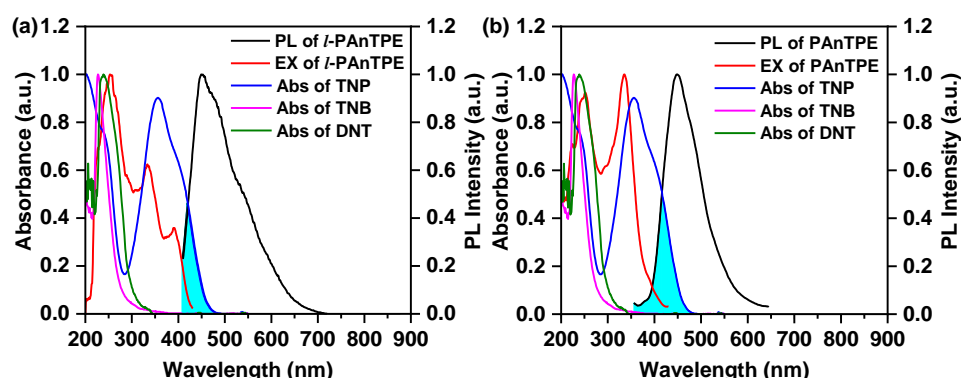

Figure 8. The excitation and PL spectra of *l*-PAnTPE (**a**) and PAnTPE (**b**), and the UV-Vis absorption spectra of TNP, TNB and DNT in water.

Furthermore, to reveal the dynamic/static mechanism of PL quenching, we studied the PL lifetimes of *l*-PAnTPE and PAnTPE aqueous dispersion upon TNP addition by time resolved PL decay experiments. As shown in Figure 9, the average PL lifetimes of *l*-PAnTPE and PAnTPE are similar, with 1.31 ns and 1.49 ns, respectively. When TNP was added, the PL lifetimes obtained from the decay curves kept almost unchanged, with 1.20 ns and 1.50 ns, respectively, indicating that the static quenching is involved in the TNP quenching mechanism. Furthermore, the ratio of τ_0/τ is plotted as a function of TNP

concentration (Figure S10), where τ_0 represents the initial average PL lifetimes of *l*-PAnTPE and PAnTPE, τ represents the average PL lifetimes at different TNP concentration. As shown in Figure S10, the plots of τ_0/τ vs. TNP concentrations are linearly fitted and parallel to the x axis, showing almost unchanged PL lifetimes before and after TNP addition, thus demonstrating that the static quenching dominates the quenching process of TNP [59]. Therefore, it can be considered that the IFT is the key reason for the remarkable sensitivity and selectivity based on *l*-PAnTPE and PAnTPE nanoparticles for TNP detection in the aqueous phase.
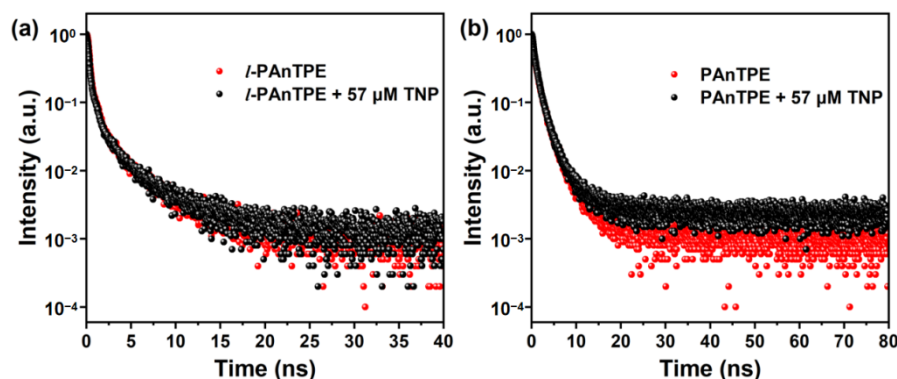

Figure 9. The lifetime decay curves of *l*-PAnTPE (**a**) and PAnTPE (**b**) in water before and after adding TNP (57 μM).

3.5. Paper Strips Tests

To realize fast, low cost and real-time TNP detection, paper strips were fabricated using our polymers. As shown in Figure 10, the paper strips coated with our polymers exhibit blue emission under the excitation of UV light at 365 nm. When different concentrations of TNP solutions were added onto paper strips, the PL of the strips were gradually quenched with the increase in TNP content. Importantly, the obvious PL quenching could be recognized with TNP concentration of only 0.05 mg/mL. The paper strips of our polymers demonstrate a potential for real-time application towards trace TNP.
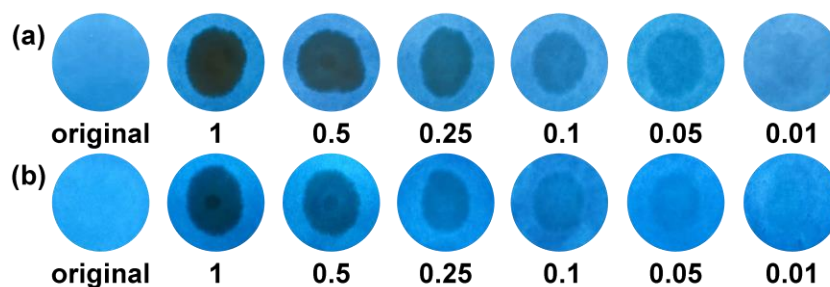

Figure 10. Paper strips of *l*-PAnTPE (**a**) and PAnTPE (**b**) before and after adding TNP solution (concentration: 0.01, 0.05, 0.1, 0.25, 0.5, 1 mg/mL, respectively).

4. Conclusions

In summary, the novel linear polymer *l*-PAnTPE and cross-linked polymer PAnTPE nanoparticles based on anthracene and tetraphenylethene were successfully synthesized by Suzuki coupling polymerization in toluene/water miniemulsion. Uniform polymer nanoparticles were prepared with particle sizes around 73 nm, which makes them well dispersed in the pure aqueous phase. The two conjugated polymers *l*-PAnTPE and PAnTPE nanoparticles could be used for the detection of nitroaromatics in aqueous media, especially for TNP, with LODs of 663 nM and 439 nM, respectively. The porous structure of the cross-linked PAnTPE is beneficial to the adsorption/diffusion of the quencher, leading to a better quenching performance towards nitroaromatics than the linear polymer

l-PAnTPE. Further investigation of sensing mechanism indicates that static quenching dominates the TNP sensing process, thus the high sensitivity and selectivity detection of TNP, compared to the other nitroaromatics could be mainly attributed to the IFT effect. In addition, the *l*-PAnTPE and PAnTPE paper strips show good sensing performance for TNP detection, thus demonstrating the great potential of *l*-PAnTPE and PAnTPE nanoparticles in practical application.

Supplementary Materials: The following supporting information can be downloaded at: https://www.mdpi.com/article/10.3390/chemosensors10090366/s1, Reagents and measurements; Figure S1: TEM images of *l*-PAnTPE (**a**) and PAnTPE (**b**); Figure S2: DLS curves of *l*-PAnTPE (**a**) and PAnTPE (**b**); Figure S3: Linear relationship between different quantities of TNP and PL intensities of polymers *l*-PAnTPE (**a**) and PAnTPE (**b**) aqueous dispersion; Figure S4: Emission spectra of *l*-PAnTPE aqueous dispersion by addition of TNB (**a**) and DNT (**c**). S–V plots of relative PL intensities ($I_0/I-1$) of *l*-PAnTPE vs. TNB (**b**) and DNT (**d**) concentration; Figure S5: Linear relationship between different quantities of explosives and PL intensity of *l*-PAnTPE aqueous dispersion; Figure S6: Emission spectra of PAnTPE aqueous dispersion by addition of TNB (**a**) and DNT (**c**). S–V plots of relative PL intensities ($I_0/I-1$) of PAnTPE vs. TNB (**b**) and DNT (**d**) concentration; Figure S7: Linear relationship between different quantities of explosives and PL intensity of PAnTPE aqueous dispersion; Figure S8: PL quenching degree of *l*-PAnTPE (**a**) and PAnTPE (**b**) aqueous dispersion by adding potential interfering ions (Na^+, K^+, Ba^{2+} and Ca^{2+} of 450 μM; Mg^{2+}, Fe^{2+}, Mn^{2+}, Zn^{2+} and OH^- of 200 μM; Fe^{3+}, Cu^{2+}, NO_2^- and Br^- of 100 μM) and TNP (70 and 35 μM in *l*-PAnTPE and PAnTPE, respectively); Figure S9: The cyclic voltammogram curves of *l*-PAnTPE (**a**) and PAnTPE (**b**) in acetonitrile; Figure S10: linear fitting of τ_0/τ of *l*-PAnTPE (**a**) and PAnTPE (**b**) vs. TNP concentration, where τ_0 is the average PL lifetime of polymer dispersion, and τ is the average PL lifetime upon TNP addition; Table S1: LODs and LOQs of *l*-PAnTPE for TNP, TNB and DNT, respectively; Table S2: LODs and LOQs of PAnTPE for TNP, TNB and DNT, respectively.

Author Contributions: T.O.: Formal analysis, Investigation, Data curation, Writing—original draft; X.G.: Formal analysis, Writing—review and editing; Q.C.: Formal analysis, Data curation; W.Z.: Formal analysis, Data curation; W.D.: Conceptualization, Funding acquisition, Project administration, Supervision, Writing—review and editing; T.F.: Conceptualization, Supervision, Writing—review and editing. All authors have read and agreed to the published version of the manuscript.

Institutional Review Board Statement: Not applicable.

Informed Consent Statement: Not applicable.

Data Availability Statement: Not applicable.

Conflicts of Interest: The authors declare no conflict of interest.

References

1. Akhgari, F.; Fattahi, H.; Oskoei, Y.M. Recent advances in nanomaterial-based sensors for detection of trace nitroaromatic explosives. *Sens. Actuators B-Chem.* **2015**, *221*, 867–878. [CrossRef]
2. Zhang, Y.; Fu, Y.-Y.; Zhu, D.-F.; Xu, J.-Q.; He, Q.-G.; Cheng, J.-G. Recent advances in fluorescence sensor for the detection of peroxide explosives. *Chin. Chem. Lett.* **2016**, *27*, 1429–1436. [CrossRef]
3. Dong, W.Y.; Fei, T.; Scherf, U. Conjugated polymers containing tetraphenylethylene in the backbones and side-chains for highly sensitive TNT detection. *RSC Adv.* **2018**, *8*, 5760–5767. [CrossRef]
4. Nabeel, F.; Rasheed, T.; Mahmood, M.F.; Salah Ud-Din, K. Hyperbranched copolymer based photoluminescent vesicular probe conjugated with tetraphenylethene: Synthesis, aggregation-induced emission and explosive detection. *J. Mol. Liq.* **2020**, *308*, 113034. [CrossRef]
5. Ma, J.; Lv, L.; Zou, G.; Zhang, Q. Fluorescent porous film modified polymer optical fiber via "click" chemistry: Stable dye dispersion and trace explosive detection. *ACS Appl. Mater. Interfaces* **2015**, *7*, 241–249. [CrossRef]
6. Aamir, M.; Irum, S.; Siddiq, A.; Batool, H.M.; Ahmed, N.; Awais, M.H.; Ali, S. A novel method development and validation for determination of 2,4,6-trinitrotoluene and its metabolites on LC-MS/MS. *Anal. Biochem.* **2022**, *638*, 114496. [CrossRef] [PubMed]

7. Shahraki, H.; Tabrizchi, M.; Farrokhpor, H. Detection of explosives using negative ion mobility spectrometry in air based on dopant-assisted thermal ionization. *J. Hazard. Mater.* **2018**, *357*, 1–9. [CrossRef]

8. Rodriguez, J.L.; Almirall, J.R. Continuous vapor sampling of volatile organic compounds associated with explosives using capillary microextraction of volatiles (CMV) coupled to a portable GC-MS. *Forensic Chem.* **2021**, *26*, 100380. [CrossRef]

9. Schachel, T.D.; Stork, A.; Schulte-Ladbeck, R.; Vielhaber, T.; Karst, U. Identification and differentiation of commercial and military explosives via high performance liquid chromatography—High resolution mass spectrometry (HPLC-HRMS), X-ray diffractometry (XRD) and X-ray fluorescence spectroscopy (XRF): Towards a forensic substance database on explosives. *Forensic Sci. Int.* **2020**, *308*, 110180.

10. González-Méndez, R.; Reich, D.F.; Mullock, S.J.; Corlett, C.A.; Mayhew, C.A. Development and use of a thermal desorption unit and proton transfer reaction mass spectrometry for trace explosive detection: Determination of the instrumental limits of detection and an investigation of memory effects. *Int. J. Mass Spectrom.* **2015**, *385*, 13–18. [CrossRef]

11. Giustina, G.D.; Sonato, A.; Gazzola, E.; Ruffato, G.; Brusa, S.; Romanato, F. SPR Enhanced molecular imprinted sol-gel film: A promising tool for gas-phase TNT detection. *Mater. Lett.* **2016**, *162*, 44–47. [CrossRef]

12. Arman, A.; Şağlam, Ş.; Üzer, A.; Apak, R. Electrochemical determination of nitroaromatic explosives using glassy carbon/multi walled carbon nanotube/polyethyleneimine electrode coated with gold nanoparticles. *Talanta* **2022**, *238*, 122990. [CrossRef] [PubMed]

13. Gao, R.; Qian, H.; Weng, C.; Wang, X.; Xie, C.; Guo, K.; Zhang, S.; Xuan, S.; Guo, Z.; Luo., L.-B. A SERS stamp: Multiscale coupling effect of silver nanoparticles and highly ordered nano-micro hierarchical substrates for ultrasensitive explosive detection. *Sens. Actuators B-Chem.* **2020**, *321*, 128543. [CrossRef]

14. Wu, J.; Fan, M.; Deng, G.; Gong, C.; Chen, K.; Luo, J.; Chiang, K.S.; Rao, Y.-J.; Gong, Y. Optofluidic laser explosive sensor with ultralow detection limit and large dynamic range using donor-acceptor-donor organic dye. *Sens. Actuators B-Chem.* **2019**, *298*, 126830. [CrossRef]

15. Dong, W.; Fei, T.; Palma-Cando, A.; Scherf, U. Aggregation induced emission and amplified explosive detection of tetraphenylethylene substituted polycarbazoles. *Polym. Chem.* **2014**, *5*, 4048–4053. [CrossRef]

16. Bogireddy, N.K.R.; Silva, R.C.; Valenzuela, M.A.; Agarwal, V. 4-Nitrophenol optical sensing with N doped oxidized carbon dots. *J. Hazard. Mater.* **2020**, *386*, 121643. [CrossRef]

17. Patil, P.D.J.; Ingle, R.D.; Wagalgave, S.W.; Bhosale, R.S.; Bhosale, S.V.; Pawar, R.P.; Bhosale, S.V. A Naphthalimide-benzothiazole conjugate as colorimetric and fluorescent sensor for selective trinitrophenol detection. *Chemosensors* **2019**, *7*, 38. [CrossRef]

18. Tümay, S.O.; Yeşilot, S. Small molecule based water-soluble fluorescence material for highly selective and ultra-sensitive detection of TNT: Design and spectrofluorimetric determination in real samples. *Sens. Actuators B-Chem.* **2021**, *343*, 130088. [CrossRef]

19. Liu, J.L.; Zabetakis, D.; Acevedo-Vélez, G.; Goldman, E.R.; Anderson, G.P. Comparison of an antibody and its recombinant derivative for the detection of the small molecule explosive 2,4,6-trinitrotoluene. *Anal. Chim. Acta* **2013**, *759*, 100–104. [CrossRef]

20. Kim, D.; Yoo, S. Aptamer-conjugated quantum dot optical biosensors: Strategies and applications. *Chemosensors* **2021**, *9*, 318. [CrossRef]

21. Wu, K.; Hu, J.; Shi, S.; Li, J.; Cheng, X. A thermal stable pincer-MOF with high selective and sensitive nitro explosive TNP, metal ion Fe^{3+} and pH sensing in aqueous solution. *Dyes Pigments* **2020**, *173*, 107993. [CrossRef]

22. Qiao, X.; Han, Y.; Tian, D.; Yang, Z.; Li, J.; Zhao., S. MOF matrix doped with rare earth ions to realize ratiometric fluorescent sensing of 2,4,6-trinitrophenol: Synthesis, characterization and performance. *Sens. Actuators B-Chem.* **2019**, *286*, 1–8. [CrossRef]

23. Ji, G.; Zheng, T.; Gao, X.; Liu, Z. A highly selective turn-on luminescent logic gates probe based on post-synthetic MOF for aspartic acid detection. *Sens. Actuators B-Chem.* **2019**, *284*, 91–95. [CrossRef]

24. Kumar, V.; Saini, S.K.; Choudhury, N.; Kumar, A.; Maiti, B.; De, P.; Kumar, M.; Satapathi, S. Highly sensitive detection of nitro compounds using a fluorescent copolymer-based FRET System. *ACS Appl. Polym. Mater.* **2021**, *3*, 4017–4026. [CrossRef]

25. Kalva, N.; Tran, C.H.; Lee, M.W.; Augustine, R.; Lee, S.J.; Kim, L. Aggregation-induced emission-active hyperbranched polymers conjugated with tetraphenylethylene for nitroaromatic explosive detection. *Dyes Pigments* **2021**, *194*, 109617. [CrossRef]

26. Mi, H.-Y.; Liu, J.-L.; Guan, M.-M.; Liu, Q.-W.; Zhang, Z.-Q.; Feng., G.-D. Fluorescence chemical sensor for determining trace levels of nitroaromatic explosives in water based on conjugated polymer with guanidinium side groups. *Talanta* **2018**, *187*, 314–320. [CrossRef]

27. Malik, A.H.; Hussain, S.; Kalita, A.; Iyer, P.K. Conjugated polymer nanoparticles for the amplified detection of nitro-explosive picric acid on multiple platforms. *ACS Appl. Polym. Mater.* **2015**, *7*, 26968–26976. [CrossRef]

28. Samukaite-Bubniene, U.; Mazetyte-Stasinskiene, R.; Chernyakova, K.; Karpicz, R.; Ramanavicius, A. Time-resolved fluorescence spectroscopy based evaluation of stability of glucose oxidase. *Int. J. Biol. Macromol.* **2022**, *163*, 676–682. [CrossRef]

29. Meng, Y.; Zhang, N.; Li, J.; Xu, Y.; Yang, Q.; Yuan, Y.; Zhang, X.; Wu, J.; Zhao, L. The detection of selectivity and sensitivity towards TNP by a new Zn(II)-coordination polymer as luminescent sensor in aqueous solution. *Spectrochim. Acta A* **2022**, *266*, 120419. [CrossRef]

30. Han, X.; Tong, J.; Ding, G.; Sun, C.; Wang, X.; Su, Z.; Sun, J.; Wen, L.-L.; Shan, G.-G. A low-dimensional N-rich coordination polymer as an effective fluorescence sensor for 2,4,6-trinitrophenol detection in an aqueous medium. *New J. Chem.* **2022**, *46*, 1551–1556. [CrossRef]

31. Zhou, Q.; Swager, T.M. Fluorescent chemosensors based on energy migration in conjugated polymers: The molecular wire approach to increased sensitivity. *J. Am. Chem. Soc.* **1995**, *117*, 12593–12602. [CrossRef]

32. Qu, Y.; Wu, Y.; Gao, Y.; Qu, S.; Yang, L.; Hua, J. Diketopyrrolopyrrole-based fluorescent conjugated polymer for application of sensing fluoride ion and bioimaging. *Sens. Actuators B-Chem.* **2014**, *197*, 13–19. [CrossRef]

33. Ramanavicius, A.; Ryskevic, N.; Kausaite-Minkstimiene, A.; Jursenas, S.; Baniukevic, J.; Kirlyte, J. Immunosensor based on fluorescence quenching matrix of the conducting polymer polypyrrole. *Anal. Bioanal. Chem.* **2010**, *398*, 3105–3113. [CrossRef] [PubMed]

34. Ma, X.-S.; Wang, D.-H.; Cui, Y.-Z.; Tao, F.-R.; Wang, Y.-T.; Li, T.-D. A novel hydrophilic conjugated polymer containing hydroxyl groups: Syntheses and sensing performance for NACs in aqueous solution. *Sens. Actuators B-Chem.* **2017**, *251*, 851–857. [CrossRef]

35. Yan, C.; Qin, W.; Li, Z.; Zhou, Y.; Cui, Y.; Liang, G. Quantitative and rapid detection of explosives using an efficient luminogen with aggregation-induced emission characteristics. *Sens. Actuators B-Chem.* **2020**, *302*, 127201. [CrossRef]

36. Zhang, C.; Pan, G.; He, Y. Conjugated microporous organic polymer as fluorescent chemosensor for detection of Fe^{3+} and Fe^{2+} ions with high selectivity and sensitivity. *Talanta* **2022**, *236*, 122872. [CrossRef]

37. Zhang, W.; Gao, B.; Guo, X.; Dong, W. Polyfluorene based fluorescent sensor for sensitive and selective detection of picric acid. *Mater. Lett.* **2022**, *306*, 130860. [CrossRef]

38. Liu, J.; Zhong, Y.; Lam, J.W.Y.; Lu, P.; Hong, Y.; Yu, Y.; Yue, Y.; Faisal, M.; Sung, H.H.Y.; Williams, I.D.; et al. Hyperbranched conjugated polysiloles: Synthesis, structure, aggregation-enhanced emission, multicolor fluorescent photopatterning, and superamplified detection of explosives. *Macromolecules* **2010**, *43*, 4921–4936. [CrossRef]

39. Sengottuvelu, D.; Kachwal, V.; Raichure, P.; Raghav, T.; Laskar, L.R. Aggregation-induced enhanced emission (AIEE)-active conjugated mesoporous oligomers (CMOs) with improved quantum yield and low-cost detection of a trace amount of nitroaromatic explosives. *ACS Appl. Mater. Interfaces* **2020**, *12*, 31875–31886. [CrossRef]

40. Wu, X.; Hang, H.; Li, H.; Chen, Y.; Tong, H.; Wang, L. Water-dispersible hyperbranched conjugated polymer nanoparticles with sulfonate terminal groups for amplified fluorescence sensing of trace TNT in aqueous solution. *Mater. Chem. Front.* **2007**, *1*, 1875–1880. [CrossRef]

41. Bandyopadhyay, S.; Pallavi, P.; Anil, A.G.; Patra, A. Fabrication of porous organic polymers in the form of powder, soluble in organic solvents and nanoparticles: A unique platform for gas adsorption and efficient chemosensing. *Polym. Chem.* **2015**, *6*, 3775–3780. [CrossRef]

42. Dong, W.; Ma, Z.; Duan, Q.; Fei, T. Crosslinked fluorescent conjugated polymer nanoparticles for high performance explosive sensing in aqueous media. *Dyes Pigments* **2018**, *159*, 128–134. [CrossRef]

43. Liang, X.; Wen, L.; Mi, Y.; Guo, J.; Yu, B.; Tao, M.; Cao, Z.; Zhao, Z. Highly cross-linked polymeric nanoparticles with aggregation-induced emission for sensitive and recyclable explosive detection. *Dyes Pigments* **2021**, *191*, 109369. [CrossRef]

44. Yao, J.; Zhuang, Z.; Yao, H.; Shi, R.; Chang, C.; Zhou, J.; Zhao, Z. Tetraphenylethene-based polymeric fluorescent probes for 2,4,6-trinitrophenol detection and specific lysosome labelling. *Dyes Pigments* **2020**, *182*, 108588. [CrossRef]

45. Zhang, H.; Zhou, J.; Shan, G.-G.; Li, G.-F.; Sun, C.-Y.; Cui, D.-X.; Wang, X.-L.; Su, Z.-M. A tetraphenylethylene-based covalent organic polymer for highly selective and sensitive detection of Fe^{3+} and as a white light emitting diode. *Chem. Commun.* **2019**, *55*, 12328–12331. [CrossRef] [PubMed]

46. Dong., J.; Zhang, K.; Li, X.; Qian, Y.; Zhu, H.; Yuan, D.; Xu, Q.-H.; Jiang, J.; Zhao, D. Ultrathin two-dimensional porous organic nanosheets with molecular rotors for chemical sensing. *Nat. Commun.* **2017**, *8*, 1142. [CrossRef] [PubMed]

47. Chen, T.; Yin, H.; Chen, Z.-Q.; Zhang, G.-F.; Xie, N.-H.; Li, C.; Gong, W.-L.; Tang, B.Z.; Zhu, M.-Q. Monodisperse AIE-active conjugated polymer nanoparticles via dispersion polymerization using Geminal cross-coupling of 1,1-dibromoolefins. *Small* **2016**, *12*, 6547–6552. [CrossRef] [PubMed]

48. Dineshkumar, S.; Laskar, I.R. Study of the mechanoluminescence and 'aggregation-induced emission enhancement' properties of a new conjugated oligomer containing tetraphenylethylene in the backbone: Application in the selective and sensitive detection of explosive. *Polym. Chem.* **2018**, *9*, 5123–5132. [CrossRef]

49. Li, B.; Hu, R.; Qin, A.; Tang, B.Z. Copper-based ionic liquid-catalyzed click polymerization of diazides and diynes toward functional polytriazoles for sensing applications. *Polym. Chem.* **2020**, *11*, 2006–2014. [CrossRef]

50. Sun, R.; Feng, S.; Zhou, B.; Chen, Z.; Wang, D.; Liu, H. Flexible cyclosiloxane-linked fluorescent porous polymers for multifunctional chemical sensors. *ACS Macro. Lett.* **2020**, *9*, 43–48. [CrossRef]

51. Kumer, V.; Maiti, B.; Chini, M.K.; De, P.; Satapathi, S. Multimodal fluorescent polymer sensor for highly sensitive detection of nitroaromatics. *Sci. Rep.* **2019**, *9*, 7269. [CrossRef] [PubMed]

52. Tanwar, A.S.; Adil, L.R.; Afroz, M.A.; Iyer, P.K. Inner filter effect and resonance energy transfer based attogram level detection of nitroexplosive picric acid using dual emitting cationic conjugated polyfluorene. *ACS Sens.* **2018**, *3*, 1451–1461. [CrossRef]

53. Giri, D.; Patra, S.K. 1,2,3-Triazolyl functionalized thiophene, carbazole and fluorene based A-alt-B type π-conjugated copolymers for the sensitive and selective detection of aqueous and vapor phase nitroaromatics (NACs). *J. Mater. Chem. C* **2020**, *8*, 14469–14480. [CrossRef]

54. Turhan, H.; Tukenmez, E.; Karagoz, B.; Bicak, N. Highly fluorescent sensing of nitroaromatic explosives in aqueous media using pyrene-linked pbema microspheres. *Talanta* **2018**, *179*, 107–114. [CrossRef] [PubMed]

55. Zhuang, Y.; Shan, H.; Zhang, Z.; Li, S.; Zhu, Q.; Si, Z.; Yang, S.; Yang, Z.; Cai, D.; Qin, P. Triazine-based covalent organic polymer as stable luminescent probe for highly selective detection of 2,4,6-trinitrophenol. *Dyes Pigments* **2021**, *192*, 109421. [CrossRef]

56. Ye, D.-Y.; Dong, Z.-Y.; Pu, Y.-Q.; Huang, G.-W.; An, Y.; Lü, L.-W. Design two large conjugate triazolopyrimidine analogs and apply them to detect 2,4,6-trinitrophenol. *Dyes Pigments* **2020**, *174*, 108016. [CrossRef]

57. Liu, G.; Abdurahman, A.; Zhang, Z.; Feng, Y.; Li, F.; Zhang, M. New three-component conjugated polymers and their application as super rapid-response fluorescent probe to DNT vapor. *Sens. Actuators B-Chem.* **2019**, *296*, 126592. [CrossRef]
58. Guo, X.; Gao, B.; Cui, X.; Wang, J.; Dong, W.; Duan, Q.; Fei, T.; Su, Z. PL sensor for sensitive and selective detection of 2,4,6-trinitrophenol based on carbazole and tetraphenylsilane polymer. *Dyes Pigments* **2021**, *191*, 109379. [CrossRef]
59. Shellaiah, M.; Awasthi, K.; Chandran, S.; Aazaad, B.; Sun, K.W.; Ohta, N.; Wu, S.-P.; Lin, M.-C. Methylammonium tin tribromide quantum dots for heavy metal ion detection and cellular imaging. *ACS Appl. Nano Mater.* **2022**, *5*, 2859–2874. [CrossRef]